CONTRAST MEDIA & MOLECULAR IMAGING

Received: 4 May 2011, Revised: 18 July 2011, Accepted: 30 July 2011, Published online in Wiley Online Library: 2012

(wileyonlinelibrary.com) DOI: 10.1002/cmmi.478

Novel Gd(III)-based probes for MR molecular imaging of matrix metalloproteinases

Concetta V. Gringeri[a], Valeria Menchise[b], Silvia Rizzitelli[c], Evelina Cittadino[c], Valeria Catanzaro[c], Gabriele Dati[d], Linda Chaabane[d], Giuseppe Digilio[a]* and Silvio Aime[c]

Two novel Gd-based contrast agents (CAs) for the molecular imaging of matrix metalloproteinases (MMPs) were synthetized and characterized *in vitro* and *in vivo*. These probes were based on the PLG*LWAR peptide sequence, known to be hydrolyzed between Gly and Leu by a broad panel of MMPs. A Gd–DOTA chelate was conjugated to the N-terminal position through an amide bond, either directly to proline (compd Gd–K11) or through a hydrophilic spacer (compd Gd–K11N). Both CA were made strongly amphiphilic by conjugating an alkyl chain at the C-terminus of the peptide sequence. Gd–K11 and Gd–K11N have a good affinity for β-cyclodextrins (K_D 310 and 670 μM respectively) and for serum albumin (K_D 350 and 90 μM respectively), and can be efficiently cleaved *in vitro* at the expected site by MMP-2 and MMP-12. Upon MMP-dependent cleavage, the CAs lose the C-terminal tetrapeptide and the alkyl chain, thus undergoing to an amphiphilic-to-hydrophilic transformation that is expected to alter tissue pharmacokinetics. To prove this, Gd–K11 was systemically administered to mice bearing a subcutaneous B16.F10 melanoma, either pre-treated or not with the broad spectrum MMP inhibitor GM6001 (Ilomastat). The washout of the Gd-contrast enhancement in MR images was significantly faster for untreated subjects (displaying MMP activity) with respect to treated ones (MMP activity inhibited). The washout kinetics of Gd-contrast enhancement from the tumor microenvironment could be then interpreted in terms of the local activity of MMPs. Copyright © 2012 John Wiley & Sons, Ltd.

Keywords: matrix metalloproteinase; gadolinium; contrast agent; MRI; tumor; mouse melanoma

1. INTRODUCTION

Matrix metalloproteinases (MMPs) are a family of zinc-dependent endoproteases that degrade proteins in the extracellular matrix (ECM) and have a key role in tissue remodeling in normal (angiogenesis, tissue repair) as well as in pathological conditions (1,2). More than 25 members of this family sharing common structural features are currently known, grouped into sub-families according to their substrate preferences (gelatinases, collagenases, stromelysins, etc). Most MMPs are excreted in the ECM as inactive zymogens and activated by cleavage of a propeptide segment, which coordinates the catalytic zinc ion through a cysteine thiol group, making it inaccessible to the substrate, while a small number of MMP members exert their function as membrane bound ectoenzymes (MT-MMP) (3). There is a growing body of evidence indicating that different pathological states are characterized by a specific pattern of MMP activity, and such a pattern may be thought of as a sort of signature of a given pathology (tumor, neurodegeneration, inflammation). In oncology the role of MMPs has been thoroughly studied and debated, and it is well established that certain members of this family, most notably gelatinases (also known as MMP-2 and MMP-9), contribute to all stages of tumor progression, including proliferation, adhesion, migration, angiogenesis and invasion. For instance, the level of MMPs expression and activity in malignant cancers is generally higher than in normal or premalignant tissues, with maximum activity occurring in areas of active invasion at the tumor–stroma interface (4,5). Glioblastoma multiforme has been associated with the upregulation of MMP-2, -9 and all MT-MMPs (6).

The assessment by clinically relevant imaging techniques (MRI or PET) of the activity of MMPs in a given anatomical microenvironment would be of great value for the classification and staging of the pathological process, and for the evaluation of the efficacy of therapies. The ideal probe for imaging MMP activity is a system that selectively accumulates within the region of interest, being silent (e.g. no contrast into images) in the regions deprived of MMP expression. Two main approaches can be followed to design a molecular imaging procedure for the detection of MMPs. Inhibitors of MMPs can be conjugated to a suitable

* *Correspondence to: G. Digilio, Department of Environmental and Life Sciences, Università del Piemonte Orientale 'A. Avogadro', Viale T. Michel 11, I-15121 Alessandria, Italy.*
E-mail: giuseppe.digilio@mfn.unipmn.it

a *C. V. Gringeri, G. Digilio*
Department of Environmental and Life Sciences, Università del Piemonte Orientale 'A. Avogadro', Viale T. Michel 11, 15121 Alessandria, Italy

b *V. Menchise*
Institute for Biostructures and Bioimages (CNR) c/o Molecular Biotechnology Center (University of Turin), Via Nizza 52, 10125 Torino, Italy

c *S. Rizzitelli, E. Cittadino, V. Catanzaro, S. Aime*
Department of Chemisty IFM and Center for Molecular Imaging, University of Turin, Via Nizza 52, 10125 Torino, Italy

d *G. Dati, L. Chaabane*
San Raffaele Scientific Institute, INSPE-Division Neuroscience, Via Olgettina 58, 20132 Milan, Italy

imaging probe, such that the labeled inhibitor will accumulate in regions where MMPs are expressed. According to this approach, several works have been published on MMP inhibitors labeled with a PET/SPECT radiotracer (7–10). Molecular MRI of MMPs has been very recently achieved with the conjugation of a Gd–DOTA complex to a broad spectrum MMP inhibitor. *In vivo* MRI in ApoE$^{-/-}$ mouse model has shown that this MRI probe accumulates within MMP-rich atherosclerotic plaques, improving detection sensitivity (11). An alternative strategy to the visualization of MMPs relies on the use of substrates of MMPs rather than inhibitors. An impressive amount of work has led to the identification of short peptide sequences that can be more or less selectively cleaved at a given peptidic bond by selected members of the MMP family (12–14). Such sequences can be conjugated to fluorophores or 'quenchers' to obtain imaging probes for FRET optical imaging, and a large collection of such probes is currently available and routinely used for preclinical assessment of MMPs activity (15). Recently, an interesting adaptation of this approach to obtain MRI contrast agents has been proposed. It relies on the use of MMP-7 (16) or MMP-2 (17,18) cleavable peptide sequences functionalized at the N-terminus with a Gd(III)–DOTA chelate. The design of the probe has been pursued to obtain a hydrophilic system when intact, whereas the fragments bearing the gadolinium unit released after enzymatic cleavage are more hydrophobic or even insoluble. The hydrophilic-to-hydrophobic transformation (solubility switch) makes the gadolinium complex less soluble (or it interacts more strongly with the hydrophobic components of the ECM), resulting in an enhanced retention time in the ECM microenvironment. Following this idea, the activity of MMP-2 in mouse tumor models has been evaluated by following the kinetics of gadolinium enhancement by MRI (16,18).

In this work we report an alternative MR-molecular imaging approach for the visualization of MMPs activity, based upon a gadolinium-based contrast agent undergoing an amphiphilic-to-hydrophilic rather than a hydrophilic-to-hydrophobic transformation. The advantage is that an amphiphilic contrast agent (CA) can be more easily inserted into nanosized carrier systems such as liposomes, making simpler and more flexible the building up of targeted carriers (19,20). Moreover, nanosized systems can in principle be loaded with therapeutics in addition to the contrast agent, opening the way to imaging guided drug delivery and 'theragnostic' approaches (21,22). In the present work, the synthesis and chemical characterization of two Gd-based probes will be described, and their ability to report on MMP activity will be assessed in a melanoma mouse model by dynamic contrast enhancement (DCE) MRI.

2. RESULTS AND DISCUSSION

2.1. Design and synthesis of the Gd(III) complexes

Two hydrophobic MMP-cleavable contrast agents for the MR molecular imaging of MMPs were synthesized (referred to as Gd–K11 and Gd–K11N, see Scheme 1). The responsive part of both probes was based upon the PLG–*LWAR peptide sequence, which is known to be efficiently cleaved at the Gly–Leu site by several MMPs and has been extensively used for MMP-responsive fluorescence probes (23–25). In Gd–K11, the Gd–DOTA unit was directly bound to the N-terminus proline of the peptide sequence through the formation of an amide bond involving one of the acetic acid arms of the chelating cage and the proline amino group. In Gd–K11N, a lnk-GVV (lnk = 8-amino-3,6-dioxaoctanoic acid) sequence was inserted between the Gd–DOTA and the

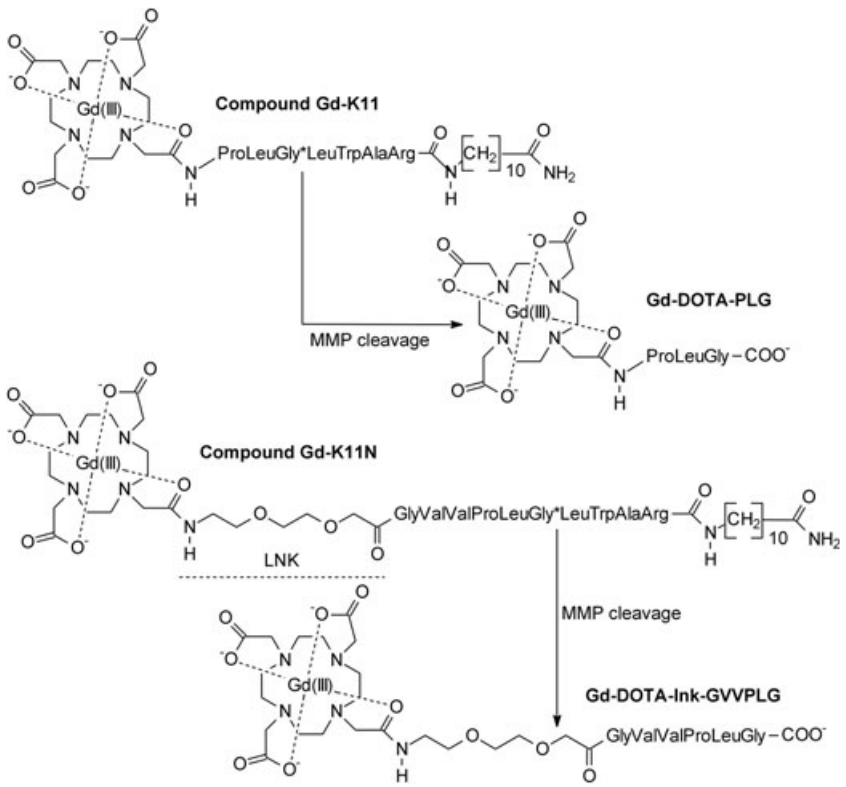

Scheme 1. Chemical structure of Gd–K11 and Gd–K11N and of the fragments released after cleavage by MMPs.

MMP-responsive sequence to enhance the amphiphilicity of the construct and to introduce a spacer between the bulky Gd-chelate and the N-terminus proline, which is known to be crucial for enzyme-substrate recognition. The C-terminus in both probes is conjugated to an alkyl chain, which has two functions. First, it makes the whole molecule more hydrophobic, such that cleavage at the expected site should rescue a Gd-containing peptide fragment having a more hydrophilic character and substantially modify tissue retention times. The second function of the alkyl chain is to provide an anchor that enables the insertion of the molecules into liposome membranes or to enable the formation of host–guest complexes with β-cyclodextrin-based nanocarriers (26,27). As a matter of fact, the work herein reported is part of a larger project aimed at building up a targeted nanomedicine based upon nanocarriers for the targeted delivery of contrast agents and MMP inhibitors.

The designed probes were amenable to solid-phase peptide synthesis (SPPS, Scheme 2). First, the alkyl chain under the form of Fmoc-protected 11-aminoundecanoic acid was linked to Rink Amide resin. The peptide chain was grown by the standard Fmoc SPPS chemistry, with 20% piperidine and PyBOP as deprotection and coupling reagents, respectively. The linkage of DOTA–tris (*tert*-butyl ester) to the proline (ligand K11) proved to be a difficult step, so that the efficiency of coupling had to be improved by repeating that step twice with increased reaction time. In the case of K11N, the insertion of the lnk-GVV strip somewhat facilitated the coupling of DOTA to the peptide. Yields around 70% could finally be obtained for both peptides, and after cleavage from the resin, deprotection and preparative HPLC purities >95% could be achieved. The complexation of the ligand with Gd(III) chloride was performed by methods published elsewhere (28,29).

2.2. ^{1}H NMR Relaxometric Characterization of the Probes

The efficacy of a Gd(III) complex as a CA for MRI applications can be summarized by a single parameter, called the millimolar relaxivity, r_1^{mM}. The relaxivity of a Gd(III) complex is defined as the enhancement of solvent water proton relaxation rate promoted by the complex at 1 mM concentration (r_1^{mM}, $mM^{-1}\ s^{-1}$):

$$R_{1obs} = R_{1p} + R_{1w} \quad (1)$$

$$R_{1p} = r_1{}^{mM}[CA] \quad (2)$$

where R_{1obs} is the measured water proton relaxation rate, R_{1p} is the paramagnetic enhancement to the water proton relaxation rate, R_{1w} the relaxation rate of pure water, and [CA] the concentration of the Gd(III) complex in mmol l^{-1}. The higher the millimolar relaxivity, the higher is the ability of a given compound to enhance image contrast. It must be emphasized that the relaxivity can be dependent upon temperature, magnetic field strength, pH and solution dynamics of the complex.

Table 1 summarizes the millimolar relaxivity of Gd–K11 and Gd–K11N measured at 25 °C, 20 MHz and in HEPES buffer pH 7.2. The larger relaxivity of Gd–K11 ($r_1^{mM} = 8.5\ mM^{-1}\ s^{-1}$) as compared

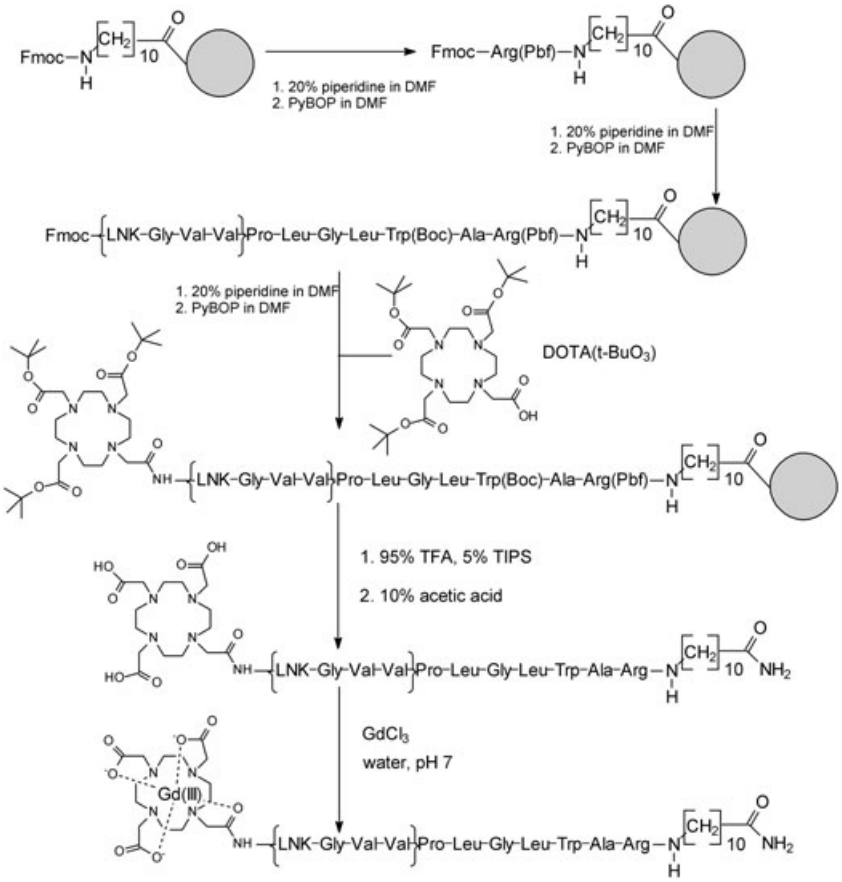

Scheme 2. Solid-phase peptide synthesis (SPPS) approach for the synthesis of Gd–K11 and Gd–K11N.

Table 1. Millimolar relaxivities r_1^{mM} of the paramagnetic probes at free and bound state and of the released fragments after cleavage by MMPs. Dissociation constants (K_D) of the probes are also reported for the interaction with serum albumin (SA) and poly-β-cyclodextrin (pBCD)

Compound	r_1^{mM} ($mM^{-1}\,s^{-1}$) 20 MHz, 25 °C	K_D (μM)
Gd–K11	8.5 ± 0.2	
Gd–K11N	5.4 ± 0.2 (at 0.3 mM) 12.7 ± 0.2 (at 5.6 mM)	
Gd–K11/pBCD	15.2 ± 0.2[a]	310 ± 50
Gd–K11N/pBCD	8.5 ± 0.4[a]	670 ± 240
Gd–K11/SA	16.3 ± 0.2[a]	350 ± 30
Gd–K11N/SA	10.3 ± 0.3[a]	90 ± 40
Gd–DOTA–PLG (from Gd–K11)	6.1 ± 0.2[b]	
Gd–DOTA–lnk–GVVPLG (from Gd–K11N)	5.1 ± 0.2[b]	

[a]Millimolar relaxivity of the complex fully bound to the macromolecule, r_{1b}.
[b]Obtained by quantitative cleavage of the parent compound by MMP-2/12.

with typical low molecular weight Gd–DOTA–monoamide complexes (around 5 $mM^{-1}\,s^{-1}$) is in line with the larger molecular size of Gd–K11 complex (30,31). The compound Gd–K11N shows a more complex and unusual behavior, since its relaxivity is almost linearly dependent upon the concentration of the complex and it cannot be uniquely defined (Fig. 1). The relaxivity of Gd–K11N increases steadily from the lower limit of 5.4 $mM^{-1}\,s^{-1}$ at 0.3 mM up to 12.7 $mM^{-1}\,s^{-1}$ at 5.6 mM (where the solution becomes rather viscous). Since the relaxivity increases without sharp changes, the formation of micelles having a well-defined size may be ruled out. The observed behavior can probably be accounted for in terms of the hydrophobic clustering of Gd–K11N into supramolecular aggregates whose average size progressively increases with the concentration of the complex. Such concentration-dependent clustering slows down the reorientation motions at the Gd(III) center, leading ultimately to the progressive increase in the millimolar relaxivity. Dynamic light scattering (DLS) measurements confirm that there is aggregation and that aggregates are polydispersed and ill-defined in terms of size and stoichiometry. Gd–K11N aggregates appear to be linked to the introduction of the lnk-GVV spacer between the Gd chelate and the MMP responsive sequence (see Scheme 1), leading to an enhanced amphiphilicity of the Gd–K11 molecule. The relaxivity of 5.4 $mM^{-1}\,s^{-1}$ measured at 0.3 mM is considerably lower than that of the Gd–K11 analogue and approaches the typical value of the DOTA–monoamide analogues.

To obtain a more detailed picture of the relaxation properties of Gd–K11N as compared with Gd–K11, nuclear magnetic resonance dispersion (NMRD) profiles of both complexes were acquired by measuring the water proton relaxation rates as a function of the applied external magnetic field. The NMRD profiles for Gd–K11 and Gd–K11N were determined at a low concentration (0.3 mM) to reduce aggregation of Gd–K11N (Fig. 2). Multiparametric fitting of these profiles according to the Solomon–Bloembergen–Morgan (SBM) theory for inner sphere paramagnetic relaxation combined with the Freed theory for the outer sphere contribution (32,33) allows one to obtain quantitative estimates of relevant parameters governing relaxation (Table 2). Since Gd–K11 and Gd–K11N are highly homogenous in their chemical structure, most relaxation parameters have similar values, and differences in their profiles can be essentially related to the correlation time for molecular tumbling (τ_R). Such parameter describes the rate at which the vector $r_{Gd\text{-}H}$ connecting the metal and the hydrogen nuclei of the coordinated water molecule reorients within the external magnetic field, and it depends to a first approximation on the molecular size of the paramagnetic system. Best fitting of the profile of Gd–K11 yielded τ_R of about 226 ps, whereas for Gd–K11N τ_R converged to 150 ps. The low τ_R found for Gd–K11N, despite its large molecular size, indicates that internal dynamics partially decouple the reorientation of the $r_{Gd\text{-}H}$ vector from overall global motions. Therefore,

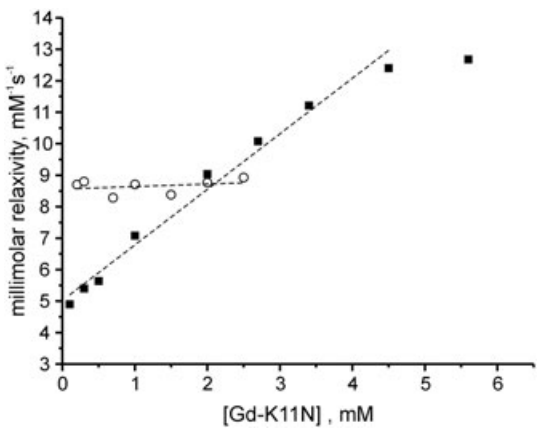

Figure 1. Plot of the millimolar relaxivity of Gd–K11N (20 MHz, 25 °C, HEPES buffer pH 7.2) as a function of the monomer concentration in the absence (black squares) and in the presence (open circles) of 52 mg ml^{-1} pBCD.

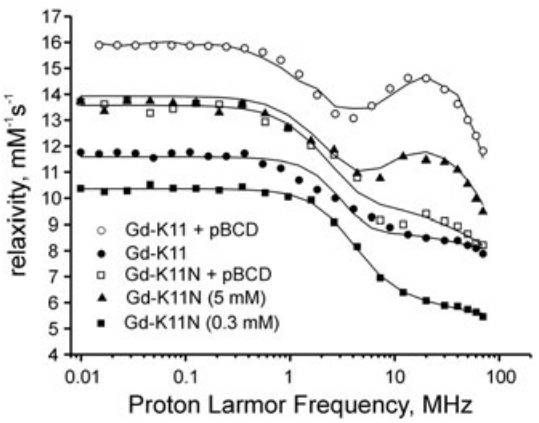

Figure 2. ^1H NMRD profiles of Gd–K11 and Gd–K11N (25 °C, HEPES buffer pH 7.2). Water proton relaxation rates are normalized against complex concentration (millimolar relaxivities). Solid circles: 0.3 mM Gd–K11. Open circles: 0.3 mM Gd–K11 in the presence of 52 mg ml^{-1} pBCD. Solid squares: 0.3 mM Gd–K11N. Open squares: 0.3 mM Gd–K11N in the presence of 52 mg ml^{-1} pBCD. Solid triangles: 5.0 mM K11N. The solid lines represent best fitting of the experimental points to the SBM theory modified according to the Lipari–Szabo model free approach (see text).

Table 2. Relaxation parameters of Gd–K11 and Gd–K11N obtained after fitting NMRD profiles to the SBM theory, combined with the LS model-free approach. For the fitting, the diffusion coefficient (D) was fixed to 2.24×10^5 cm^2 s^{-1}, the distance between Gd(III) and the inner sphere water protons (r) to 3.1 Å, their number of inner sphere water molecules q to 1, the residence lifetime (τ_M) of the inner sphere water molecule to 600 ns and the distance of closest approach of outer-sphere water protons to 3.8 Å

Probe	τ_R (ps)	S^2	Δ^2 ($s^{-2}/10^{19}$)	τ_v (ps)
K11 (0.3 mM)	226 ± 4		1.5 ± 0.1	41.8 ± 2.9
K11 + pBCD	$\tau_L = 339 \pm 144$ $\tau_G = 2250 \pm 890$	0.40 ± 0.14	0.46 ± 0.07[a]	73.9 ± 3.6[a]
K11N (0.3 mM)	$\tau_L = 141 \pm 10$ $\tau_G = 260 \pm 10$	0.39 ± 0.01	1.7 ± 0.1	30.8 ± 2.0
K11N (5 mM)	$\tau_L = 156 \pm 32$ $\tau_G = 1780 \pm 250$	0.40 ± 0.01	0.60 ± 0.06[a]	60.4 ± 3.1[a]
K11N + pBCD	$\tau_L = 220 \pm 10$ $\tau_G = 2050 \pm 150$	0.18 ± 0.07	0.68 ± 0.09[a]	56.8 ± 7.3[a]

[a]The electronic relaxation parameters Δ^2 and τ_v lose their original physical significance in large macromolecular systems endowed with faster local motions and are treated as global fitting parameters (35).

the low relaxivity of monomeric Gd–K11N can be explained by the high flexibility of the PEG-like linker that makes the local reorientation of the Gd–DOTA monoamide moiety somewhat independent from the overall molecular tumbling. As predicted by the theory, the differences of relaxivity between Gd–K11 and Gd–K11N are mostly pronounced in the 20–40 MHz region of the profile, where τ_R represents a major contribution to the observed relaxivity.

The NMRD profile of Gd–K11N acquired at a high concentration (5 mM) is clearly different from that observed at 0.3 mM, as a peak of relaxivity centered at around 20–40 MHz appears. This relaxivity peak is a clear-cut evidence of the formation of slowly tumbling supramolecular aggregates, leading to a substantial lengthening of the reorientation correlation time τ_R. This relaxivity peak was strongly attenuated at 55 °C (data not shown), indicating either some degree of de-aggregation and/or an increase of local mobility of the Gd(III) center within the aggregates. The best-fitting algorithm based upon the standard SBM theory failed to converge and no reasonable set of best-fit values could be obtained for 5 mM Gd–K11N. The reason for this is that, being the Gd–DOTA–monoamide moiety spaced from the bulk peptide by a flexible linker, the reorientation dynamics of the $r_{Gd\text{-}H}$ can not be described by a single averaged correlation time. Therefore the profile of 5 mM Gd–K11N has been fitted by the SBM model modified according to the Lipari–Szabo (LS) model free approach to get a more accurate estimation of reorientation dynamics (34,35). This model is generally used for large molecular systems whose motions can be more appropriately described through a combination of faster local motions (governed by the correlation time τ_L) and a global, slower isotropic reorientation (governed by the correlation time τ_G). The amplitude of internal motions is determined by the squared order parameter (S^2) that can range from unity (fully restricted internal motions) to zero (unrestricted motions). Following this approach, the NMRD profile could be well modeled by $\tau_L = 156$ ps and $\tau_G = 1780$ ps, with $S^2 = 0.4$. When aggregated, the overall reorientation time of Gd–K11N decreases by an order of magnitude with respect to the unaggregated state. Such a slowing down of global motions makes the relaxivity peak appear, although partially 'quenched' because of the unfavorable combination of local motions at the Gd chelate and slow exchange of the coordinated water molecule, as previously reported for related Gd–DOTA monoamide moieties (30,31).

The interactions stabilizing the supramolecular adducts of Gd–K11N probably involve the side chains of hydrophobic amino acids and the C-terminal alkyl chain of the probe. Such an alkyl chain can in principle also interact with β-cyclodextrins to form host–guest complexes. As a matter of fact, the relaxivity of Gd–K11N in the presence of >100-fold excess (as cavities) of poly-β-cyclodextrin (pBCD) remains constant with the probe concentration (Fig. 1), indicating that the formation of Gd–K11N/pBCD adducts can completely abolish self-aggregation of Gd–K11N. Titration of Gd–K11N 0.3 mM with pBCD afforded a binding curve that, best-fitted to the equation describing the binding equilibrium (36), afforded a K_D of 670 μM (Table 1). Gd–K11 also interacts with pBCD, with dissociation constant of the same order of magnitude. The NMRD profile of the Gd–K11N/β-cyclodextrin inclusion complex as compared with that of Gd–K11 (Fig. 2) does not show any relaxivity peak, confirming the different internal dynamics at the paramagnetic center in the two compounds.

For *in vivo* application and to have indications on biodistribution and pharmacokinetics, the interaction of the CAs with serum albumin (SA), representing the most abundant endogenous molecule of blood plasma, was evaluated. Therefore 0.2 mM solutions of the probes have been mixed with increasing amounts of albumin (up to 2.0 mM) in PBS at pH 7.2 and the observed relaxivity plotted against albumin concentration. The binding curves so obtained have been best-fitted by assuming one binding site per albumin molecule to obtain dissociation constants and relaxivities of the bound complex (r_{1b}), as listed in Table 1. Gd–K11N shows a very high affinity for serum albumin ($K_D = 90 \pm 40$ μM), whereas Gd–K11 has a lower but still significant affinity ($K_D = 350 \pm 30$ μM). On this basis we can predict that, in blood, a significant fraction of the compounds will be under the form of albumin complexes which will influence the biodistribution by increasing the intravascular retention.

2.3. Cleavage of the Probes by Matrix Metalloproteinases

The recognition and cleavage of the probes by MMPs have been assessed by incubating the probes with 400 nM MMP-2-9-12 for 4 h at 25 °C and by analyzing the reaction mixture by reverse-

phase HPLC-MS. For Gd–K11N, two new chromatographic peaks were found with retention times of 16.2 and 22.3 min, assigned by means of ESI-MS analysis to the Gd–DOTA–lnk–GVVPLG and H_2N–LWAR–C11–$CONH_2$ fragments, respectively (see Table 3). The shorter chromatographic retention time of Gd–DOTA–lnk–GVVPLG with respect to that of the parent compound (25.1 min) indicates that the former species is less hydrophobic, as expected, because of the release of the C-terminal alkyl chain. All MMPs considered cleaved the probe at the Gly–Leu site, as expected (see Scheme 1). Under the same experimental conditions, Gd–K11 was cleaved by MMP-2-9-12 into two fragments corresponding to H_2N–LWAR–C11–$CONH_2$ and Gd–DOTA–PLG (Table 3). No fragments corresponding to the cleavage at a site other than Gly–Leu were found.

Given the very high specificity of the cleavage site, the relaxivity of the fragments bearing the Gd(III) complex released after enzymatic cleavage were measured by following the change in relaxivity of 0.5 mM solutions of the probe in the presence of 0.4 μM MMP-2 or MMP-12 (complete hydrolysis was checked by HPLC-MS). The fragments Gd–DOTA–lnk–GVVPLG (from Gd–K11N) and Gd–DOTA–PLG (from Gd–K11) had millimolar relaxivities (r_1^{mM}) of 5.1 and 6.1 $mM^{-1}\,s^{-1}$, respectively. The decrease in relaxivity observed after hydrolysis of Gd–K11 was consistent with the decrease in the molecular mass of the compound. On the other hand, the change in relaxivity on going from Gd–K11N to its fragment was very small, because of (i) the small change of molecular weight after cleavage and (ii) the 'quenching' of the macromolecular effect owing to the internal dynamics at the Gd center (see above).

2.4. Evaluation of MMP Activity in B16 Mouse Melanoma Tumor Models

The concept for MMP activity detection based upon the differential washout kinetics of gadolinium as a function of enzymatic cleavage of the molecular probe was tested on the B16 mouse melanoma tumor model. This tumor model is widely employed to study the anti-tumoral activity of several broad spectrum MMP inhibitors (37). Six C57BL/6 mice received subcutaneously in the right flank 8×10^5 B16.F10 melanoma cells. After 7–10 days from inoculation, mice developed tumors with a diameter of 5–8 mm. In a first sub-group of animals (control group, $n = 3$), T_{1w} spin-echo MR axial images were acquired at 1 T prior and up to 3 h post the administration of Gd–K11 in the tail vein at a dose of 0.03 mmol kg^{-1} (Fig. 3). Within the tumor, the signal enhancement (SE%, normalized to the maximum signal enhancement set at 100%) started to decrease steadily with time immediately after the first acquired image, and was considerably reduced post 2 h. A second group of animals (treated group, $n = 2$) was treated with intratumor injection of a broad spectrum MMP inhibitor GM6001 (ilomastat) (38) at a dose of 8 mg kg^{-1}. This treatment with ilomastat was carried out about 15 min prior to i.v. administration of Gd–K11 to give time to the MMP inhibitor to diffuse within the tumor. The decrease of signal enhancement with time was slower compared with the control group, indicating a longer residence lifetime of gadolinium within the tumor. Thus, the washout kinetics of gadolinium differed from that of treated/untreated tumors. When MMPs were not inhibited (control), the probe was progressively cleaved and the most hydrophobic moiety (including the alkyl chain) was lost. The Gd–DOTA–PLG fragment that was released was more hydrophilic than the parent compound and its interaction with the hydrophobic components of the extracellular matrix was weak. Therefore, its washout from tumor was relatively fast. If MMPs were inhibited by means of ilomastat, the conversion of Gd–K11 into the smaller and more hydrophilic fragment was slowed down or abolished. Being Gd–K11 amphiphilic, it could interact with the hydrophobic components of the ECM, resulting in a longer retention time within tumor.

It must be recorded that Gd–K11 had severe adverse effects, especially if administered at high dose (0.1 mmol kg^{-1}), and this was the reason why the dose was reduced to 0.03 mmol kg^{-1} in the MRI assays described above. The low dose of the contrast agent was the cause of the large uncertainty appearing in the plot of Fig. 3(B). Evident clinical signs of toxicity were observed a few minutes post i.v. injection, with a progressive decrease in the respiration rate. Mice treated with 0.03 mmol kg^{-1} mostly recovered from this respiratory distress, whereas most of the subjects treated with higher doses died within 2 h post injection. Hemolysis tests done *in vitro* were negative. We suspect that the probe may aggregate, leading to breathing impairment. In addition, it has been observed with other amphiphilic cationic peptides that histamine can be released, leading to respiratory failure (39,40). Preliminary experiments in mice with Gd–K11N gave similar problems, which were slightly attenuated by decreasing the dose. We also observed that Gd–K11 and Gd–K11N accumulate in the liver eventually, because of their strong binding to albumin, and even more markedly in the kidneys, with a very slow clearance towards the bladder. However, kidney

Table 3. Qualitative analysis by RP-HPLC-MS of the fragments released by Gd–K11 and Gd–K11N after hydrolysis by MMP-2 (see also Scheme 2). RP-HPLC was carried out on a C_{18} column with gradient elution (H_2O–0.1% TFA and CH_3CN–TFA 0.1%)

Probe	Fragment released	M_w calcd	Retention time (min)	*m/z* Found	*m/z* Calcd
Gd–K11		1535.0	24.2	768.2 $[M+2H]^{2+}$	768.5
+ MMP-2	Gd–DOTA–PLG	826.05	7.0	827.0 $[M+H]^{+}$	827.05
				414.2 $[M+2H]^{2+}$	414.0
	H_2N–LWAR–C11–$CONH_2$	727.0	22.9	727.5 $[M+H]^{+}$	728.0
				364.4 $[M+2H]^{2+}$	364.5
Gd–K11N		1935.5	25.1	968.8 $[M+2H]^{2+}$	968.8
				645.9 $[M+3H]^{3+}$	646.2
+ MMP-2	Gd–DOTA–lnk–GVVPLG	1226.5	16.2	614.2 $[M+2H]^{2+}$	614.3
	H_2N–LWAR–C11–$CONH_2$	727.0	22.3	727.5 $[M+H]^{+}$	728.0
				364.4 $[M+2H]^{2+}$	364.5

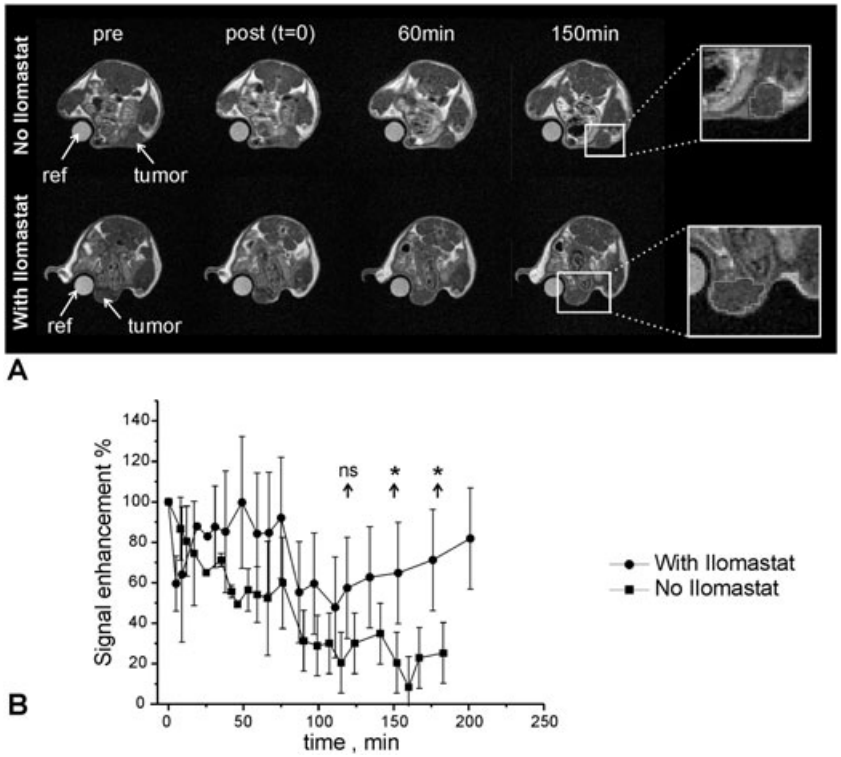

Figure 3. (A) Pre-contrast and post-contrast (Gd–K11 at 0.03 mg kg^{-1}) T_{1w}-SE axial images at 1 T in mice subcutaneously grafted with a B16 tumor treated or not with the broad spectrum MMP inhibitor ilomastat. Inserts show a magnification of the tumor area. (B) Time course of the signal enhancement (SE) in the tumor region measured after intravenous administration of 0.03 mmol kg^{-1} of Gd–K11 without (control group, $n = 3$, squares) and with (treated group, $n = 2$, circles) pre-treatment of the tumor with 8 mg kg^{-1} ilomastat. The SE is expressed as a percentage normalized to the SE measured at $t = 0$, representing the time at which the first post-contrast image has been taken. Error bars represent $\pm$ SD. Arrows indicate Student's *t*-test statistical analysis at selected time points post injection of Gd–K11 (120, 150 and 180 min; ns indicates $p > 0.05$; * $p < 0.05$).

toxicity linked with gadolinium release did not appear to be a major issue, because of the well-established high stability of Gd–DOTA monoamide chelates and because symptoms are more indicative of respiratory distress.

3. CONCLUSION

The first approach to the development of MMP-responsive contrast agents to appear in the literature was based on the exploitation of a hydrophilic-to-hydrophobic transition (16). There, a hydrophilic peptidic substrate for MMP-7 containing a Gd(III) chelate at the N-terminus and a small PEG chain at the C-terminus of the peptide was synthesized. This contrast agent was tested *in vivo* in mice bearing a human colon cancer, where MMP-dependent cleavage induced the removal of the PEG chain and a change in the pharmacokinetic profile of the CA. With respect to the intact form, an enhanced retention (slow washout) of the hydrophobic form of the contrast agent was observed and accounted for in terms of a decreased solubility of the cleaved CA, which then accumulated within the tumor. Analogous contrast agents were then developed, specifically responsive to MMP-2, showing an analogous change in the pharmacokinetics (17,18). In the present work, we proposed a different approach for the molecular imaging of MMPs, with a responsive CA undergoing a 'reverse' transition, i.e. an amphiphilic-to-hydrophilic transition. The decrease in signal enhancement within tumor was slow for the hydrophobic form (intact CA) and fast for the hydrophilic form (cleaved CA, formed when MMPs are active). Consistently with previous observations, the washout kinetics of hydrophobic CAs was slower than that of hydrophilic ones.

Given the high affinity for albumin, we can speculate that Gd–K11 can extravasate into the ECM within the tumor as an albumin complex. The long-lasting retention of Gd–K11 within tissues is most likely due to its interactions with the hydrophobic components in the ECM. In support of this view, there are well-documented examples of other Gd-containing amphiphilic CA, most notably gadofluorine M (Gf, Shering AG). Gf is composed of a Gd–DOTA–amide chelate conjugated to a perfluoroalkyl chain and shares some properties with our probes as: (i) it aggregates (micelles), but not in presence of β-cyclodextrins (41); and (ii) it has a very high affinity for serum albumin (42). It has been shown that Gf can extravasate as albumin complex and then it accumulates in the ECM, where it dissociates from albumin and binds to extracellular fibrous proteic structures (such as collagens, proteoglycans and tenascin) but not to lipidic components (40). Unlike Gf, Gd–K11 can be cleaved by proteases, thus releasing the more hydrophilic Gd–PLG fragment. Thus, the interaction with the hydrophobic components of the ECM is greatly reduced, resulting in faster washout.

In conclusion, we have presented two novel Gd-based contrast agents that can be cleaved at a specific position by matrix metalloproteinases. As a consequence of the enzymatic cleavage, the Gd-probe undergoes an amphiphilic-to-hydrophilic transformation that finally results into an alteration of the pharmacokinetic profile.

Washout kinetics from the tumor microenvironment of Gd-contrast enhancement can then be related to the local activity of MMPs.

4. EXPERIMENTAL

4.1. Synthesis of Gd–K11 and Gd–K11N

Reagents and solvents for SPPS were purchased from ABI Chemicals (Seveso, MI, Italy), Rink Amide resin was received from Merck Chemicals Ltd (Nottingham, UK). All other reagents, including Fmoc-protected amino acids, were received from Sigma-Aldrich (Milan, Italy). DOTA–tris(*tert*-butyl ester) was purchased from CAGE Chemicals (Novara, Italy).

4.1.1. Fmoc protected 11-aminoundecanoic acid

11-Aminoundecanoic acid (2.0 g; 0.010 mol) was suspended in acetone–water 1:1 and $NaHCO_3$ (0.84 g; 0.010 mol), and added under stirring with N-(9-fluorenylmethoxycarbonyloxy)-succinimide (3.37 g; 0.010 mol). The reaction mixture was stirred under inert atmosphere overnight, then acidified to pH 2 with concentrated HCl. Acetone was removed by evaporation and, after extraction with dichloromethane (3×100 ml), several washings with HCl 0.1 M (3×50 ml) and then water (3×50 ml) were done. The product was finally dried to obtain a pale yellow solid (3.77 g; 0.0089 mol) with a yield of 89%. ESI-MS $[M + Na]^+$: calcd, 446.16; found, 446.39. ^{1}H-NMR ($CDCl_3$): 7.64 ppm (d, 2H), 7.59 ppm (d, 2H), 7.40 (t, 2H), 7.31 ppm (t, 2H), 4.75 ppm (br, 1H) 4.40 ppm (d, 2H), 4.22 ppm (t, 1H), 3.18 ppm (br, 2H), 2.34 ppm (t, 2H), 1.63 ppm (m, 2H), 1.50 ppm (br, 2H), 1.4 ppm (br, o, 12H).

4.1.2. Gd–K11 and Gd–K11N

The K11N ligand was prepared by solid-phase peptide synthesis (SPPS) on an automated peptide synthesizer (CEM Liberty automated microwave peptide synthesizer) equipped with a microwave reactor. Fmoc-protected 11-aminoundecanoic acid was linked to Rink Amide resin (loading 0.5 mmol g^{-1}), then the sequence PLGLWAR or link-GVVPLGLWAR was attached stepwise to the 11-aminoundecanoic acid moiety using the standard Fmoc chemistry, with 0.5 M PyBOP in DMF as the coupling agent and 20% piperidine in DMF to release the Fmoc protection groups. The spacer (Fmoc-8-amino-3,6-dioxaoctanoic acid, Chem Impex International Inc., Wood Dale, IL, USA) was inserted through the same chemistry. The last step of the solid-phase synthesis was the coupling with DOTA–tris(*tert*-butyl ester) by performing the coupling step twice. Cleavage from the resin was accomplished by 95% trifluoroacetic acid (TFA) and 5% triisopropylsilane, and final deprotection of tryptophan was achieved by treatment with 10% acetic acid overnight at room temperature. The yield was typically around 70%. The compound was purified by RP chromatography (Atlantis® Prep C_{18}, OBD™, 5 μm particle size) on a gradient of H_2O–0.1% TFA and CH_3CN–TFA 0.1% as the eluents. The purity and identity of the compound was assessed by HPLC-ESI-MS, (Waters; 515 HPLC pump-3100 mass detector, Atlantis RP C_{18} column 4.6 × 150 mm 5 μm particle size, gradient elution with H_2O–0.1% TFA and CH_3CN–TFA 0.1%). ESI-MS for ligand K11 (M_w 1380.3): $[M+2H]^{2+}$ found 691.4 (calcd 691.2) and $[M+3H]^{3+}$ found 461.4 (calcd 461.1). For ligand K11N (M_w 1780.7): $[M+]^{2+}$ found 891.5 (calcd 891.4) and $[M+3H]^{3+}$ found 594.8 (calcd 594.6).

The Gd(III) complexes were obtained as described in Diglio *et al*. (28). Briefly, 0.95 equivalents of $GdCl_3$ were added dropwise to the ligand dissolved in water, checking the absence of free Gd(III) by means of the xylenol orange test. The complexes were finally freeze-dried to obtain a white powder. Analytical HPLC-MS was carried out for further purity check (Atlantis® RP C_{18} column 4.6 × 150 mm 5 μm particle size, gradient elution with H_2O–0.1% TFA and CH_3CN–TFA 0.1%). Gd–K11 (calcd $M_w = 1535.05$) eluted at a retention time of 23.9 min and gave an ESI-MS (positive ion detection mode) peak at $m/z = 768.2$ (corresponding to $[M+2H]^{2+}$; calcd 768.5). For Gd–K11N (calcd $M_w = 1935.46$), the retention time was 25.0 min; ESI-MS peaks at $m/z = 968.8$ (968.8 calcd) and $m/z = 645.9$ (646.2 calcd), corresponding to the $[M+2H]^{2+}$ and $[M+3H]^{3+}$ ions, respectively.

4.2. Relaxometric Characterization and Enzymatic Assay

4.2.1. ^{1}H relaxation rate measurements and NMRD profiles

The longitudinal water proton relaxation rate was measured using a Stelar Spinmaster (Stelar, Mede, Pavia, Italy) spectrometer operating at 20 MHz, by means of the standard inversion–recovery sequence. The temperature was controlled with a Stelar VTC-91 air-flow heater equipped with a copper constantan thermocouple (uncertainty 0.1 °C). Typical experimental settings included: acquisition field 9.5 MHz, 16 averaged transients, 16 data points for each T_1 measurement, and relaxation delay 2 s. The proton R_1 (= $1/T_1$) NMRD profiles were measured over a continuum of magnetic field strength from 0.00024 to 0.47 T (corresponding to 0.01–20 MHz proton Larmor frequency) on a Stelar field-cycling relaxometer. The relaxometer worked under complete computer control with an absolute uncertainty in $1/T_1$ of ±1%. Data points from 0.47 T (20 MHz) to 1.7 T (70 MHz) were collected on a Stelar Spinmaster spectrometer working at adjustable field. Typical experimental settings included: acquisition field 9.5 MHz, 16 averaged transients, 16 data points for each T_1 measurement and relaxation delay 2 s.

4.2.2. Cleavage by MMPs

MMP-2, MMP-9 and MMP-12 were purchased from either ProtEra srl (Florence, Italy) or Sigma-Aldrich (Milan, Itlay). The enzymatic cleavage of the probes was followed by virtue of the change with time of the relaxation rate (20 MHz and 25 °C) of 0.5 mM solutions (HEPES buffer pH 7.2) of the CA. A total volume of 100 μl was incubated at 25 °C for up to 24 h with 0.4 μM MMP-2, MMP-9 or MMP-12. To assess the cleavage site, the products of enzymatic cleavage after 24 h incubation time were identified by HPLC-ESI-MS (Waters; 515 HPLC pump-3100 mass detector, Atlantis RP C_{18} column 4.6 × 150 mm, 5 μm particle size, gradient elution with H_2O–0.1% TFA and CH_3CN–TFA 0.1%).

4.3. Animal Studies

All animal studies were performed according to the national regulations and were approved by the local animal experiments ethical committee. Male C57BL/6 mice (6–8 weeks of age) were obtained from Charles River Laboratories (Calco, Italy) and kept in standard housing with standard rodent chow and water available *ad libitum*, and a 12 h light–dark cycle. B16.F10 murine melanoma were cultured as monolayers at 37 °C in a 5% CO_2-containing humidified atmosphere in RPMI 1640 culture medium supplemented with 100 U ml^{-1} penicillin, 100 U ml^{-1}

streptomycin and 10% FBS. For tumor induction, 1×10^6 B16.F10 melanoma cells in 0.2 ml PBS were inoculated subcutaneously (s.c.) in the right flank of C57Bl/6 mice. Around one week after B16.F10 injection, mice developed a solid tumor of 5–8 mm in diameter and were used for MRI.

Prior to the acquisition of MR images, mice were anesthetized by administration of 20 mg kg^{-1} tiletamine–zolazepam (Zoletil 100; Virbac, Milan, Italy) mixed with 5 mg kg^{-1} xylazine (Rompun; Bayer, Milan, Italy). Intravenous injections of the CA were carried out through a catheter placed in the tail vein (200 µl of 3.0 mM solution of the CA in saline, corresponding to a dose of 0.03 mmol kg^{-1}). The broad spectrum MMP inhibitor ilomastat, also known as GM6001 or *N*-[(2*R*)-2-(hydroxamidocarbonylmethyl)-4-methylpentanoyl]-L-tryptophan methylamide was purchased from Chemicon International Inc. Ilomastat was dissolved in one drop of dimethylsulfoxide and diluted to the desired concentration with PBS. Ilomastat was injected (20 µl at 10 mg ml^{-1}) directly into the tumor about 15 min before the administration of the CA. MR images after intra tumor administration of either ilomastat or the vehicle the CA were acquired at 1 T by means of an Aspect M2-High Performance MRI System (Aspect Magnet Technologies Ltd, Netanya, Israel), mounting a NdFeB permanent magnet with a field homogeneity of 0.2–0.5 gauss. This system was equipped with a 35 mm solenoid Tx/Tr coil (inner diameter 35 mm) and fast gradient coils (gradient strength, 450 mT m^{-1} at 60 A; ramp time, 250 µs at 160 V). These MR images were acquired using a T_1-weighted spin echo sequence, *TR*/*TE*/NEX (repetition time/echo time/number of experiments) 250/7 ms/10, field of view (FOV) = 3.5 × 3.5 cm, matrix 128 × 128, slice thickness 1 mm, 20 slices. To assess CA biodistribution, MR images were also acquired on a 7 T NMR spectrometer (Bruker Avance300) equipped with a microimaging probe (birdcage resonator with 10 mm inner diameter). A T_1-weighted multislice multiecho fat-suppressed sequence was used with *TR*/*TE*/NEX = 250/3.2 ms/6, FOV 3.0 × 3.0 cm, data matrix 128 × 128, five slices each having 1.0 mm thickness. The mean signal intensity (SI) over a region of interest (ROI) manually drawn on the whole tumor was measured in three adjacent slices. These SIs were normalized against those measured for the standard Gd solution placed close to the animal (reference ROI). The signal enhancement (SE) in each slice covering the tumor was calculated according to the following equation:

$$SE = \frac{SI_{POST} - SI_{PRE}}{SI_{PRE}} \times 100$$

where SI_{PRE} and SI_{POST} are the MR signal intensity (both normalized with respect to the SI of the reference) before and after the injection of the CA.

Acknowledgements

The authors gratefully acknowledge Dr Stefania Lanzardo and Mr Franco Fedeli for technical assistance and helpful discussion. Economic and scientific support from Meditrans (Targeted Delivery of Nanomedicine: NMP4-CT-2006-026668), EU-FP7-HEALTH-2007-1.2-4 ENCITE (European Network for Cell Imaging and Tracking Expertise) and Regione Piemonte (Converging Technologies BIO-THER project; POR-FESR 2007–2013 'Piattaforme Innovative', PIIMDMT project) is gratefully acknowledged.

REFERENCES

1. Nagase HH, Woessner JF Jr. Matrix metalloproteinases. J Biol Chem 1999; 274(31): 21491–21494.
2. Massova I, Kotra LP, Fridman R, Mobashery S. Matrix metalloproteinases: structures, evolution, and diversification. FASEB J 1998; 12: 1075–1095.
3. Sounni NE, Janssen M, Foidart JM, Noel A. Membrane type-1 matrix metalloproteinase and TIMP-2 in tumor angiogenesis. Matrix Biol 2003; 22: 55–61.
4. Sternlicht MD, Bergers G. Matrix metalloproteinases as emerging targets in anticancer therapy: status and prospects. Emerging Ther Targets 2000; 4: 609–633.
5. Deryugina EI, Quigley JP. Matrix metalloproteinases and tumor metastasis. Cancer Metastasis Rev 2006; 25: 9–34.
6. Lampert K, Machein U, Machein MR, Conca W, Peter HH, Volk B. Expression of matrix metalloproteinases and their tissue inhibitors in human brain tumors. Am J Pathol 1998; 153: 429–437.
7. Van de Wiele C, Oltenfreiter R. Imaging probes targeting matrix metalloproteinases. Cancer Biother Radiopharm 2006; 21(5): 409–417.
8. auf dem Keller U, Bellac CL, Li Y, Lou Y, Lange FP, Ting R, Harwig C, Kappelhoff R, Dedhar S, Adam MJ, Ruth TJ, Bénard F, Perrin DM, Overall CM. Novel MMP inhibitor [^{18}F]-Marimastat-aryltrifluoroborate as a probe for in vivo PET imaging in cancer. Cancer Res 2010; 70(19): 7562–7569.
9. Wagner S, Breyholz H-J, Höltke C, Faust A, Schober O, Schäfers M, Kopka K. A new ^{18}F-labelled derivative of the MMP inhibitor CGS27023A for PET: radiosynthesis and initial small-animal PET studies Applied Radiat Isotopes 2009; 67: 606–610.
10. Wagner S, Breyholz H-J, Law MP, Faust A, Höltke C, Schröer S, Haufe G, Levkau B, Schober O, Schäfers M, Kopka K. Novel fluorinated derivatives of the broad-spectrum MMP inhibitors N-hydroxy-2(R)-[[(4-methoxyphenyl)sulfonyl](benzyl)- and (3-picolyl)-amino]-3-methyl-butanamide as potential tools for the molecular imaging of activated MMPs with PET. J Med Chem 2007; 50: 5752–5764.
11. Lancelot E, Amirbekian V, Brigger I, Raynaud J-S, Ballet S, David C, Rousseaux O, Le Greneur S, Port M, Lijnen HR, Bruneval P, Michel J-B, Ouimet T, Roques B, Amirbekian S, Hyafil F, Vucic E, Gilberto J, Aguinaldo S, Corot C, Fayad ZA. Evaluation of matrix metalloproteinases in atherosclerosis using a novel noninvasive imaging approach. Arterioscler Thromb Vasc Biol 2008; 28: 429–436.
12. Turk BE, Huang LL, Piro ET, Cantley LC. Determination of protease cleavage site motifs using mixture-based oriented peptide libraries. Nature Biotechnol 2001; 19: 661–667.
13. Kridel SJ, Chen E, Kotra LP, Howard EW, Mobashery S, Smith JW. Substrate hydrolysis by matrix metalloproteinase-9. J Biol Chem 2001; 276(23): 20572–20578.
14. Chen EI, Kridel SJ, Howard EW, Li W, Godzik A, Smith JW. A unique substrate recognition profile for matrix metalloproteinase-2. J Biol Chem 2002; 277(6): 4485–4491.
15. Scherer RL, McIntyre JO, Matrisian LM. Imaging matrix metalloproteinases in cancer. Cancer Metastasis Rev 2008; 27: 679–690.
16. Lepage M, Dow WC, Melchior M, You Y, Fingleton B, Quarles CC, Pepin C, Gore JC, Matrisian LM, McIntyre JO. Noninvasive detection of matrix metalloproteinase activity in vivo using a novel MRI contrast agent with a solubility switch. Mol Imag 2007; 6: 393–403.
17. Jastrzebska B, Lebel R, Therriault H, McIntyre JO, Escher E, Guerin B, Paquette B, Neugebauer WA, Lepage M. New enzyme-activated solubility-switchable contrast agent for magnetic resonance imaging: from synthesis to in vivo imaging. J Med Chem 2009; 52: 1576–1581.
18. Lebel R, Jastrzebska B, Therriault H, Cournoyer M-M, McIntyre JO, Escher E, Neugebauer W, Paquette B, Lepage M. Novel solubility-switchable MRI agent allows the noninvasive detection of matrix metalloproteinase-2 activity in vivo in a mouse model. Magn Reson Med 2008; 60: 1056–1065.
19. Mulder WJM, Strijkers GJ, Griffioen AW, van Bloois L, Molema G, Storm G, Koning GA, Nicolay K. A liposomal system for contrast-enhanced magnetic resonance imaging of molecular targets. Bioconjug Chem 2004; 15: 799–806.
20. Mulder WJM, Strijkers GJ, van Tilborg GAF, Griffioen AW, Nicolay K. Lipid-based nanoparticles for contrast-enhanced MRI and molecular imaging. NMR Biomed 2006; 19: 142–164.
21. Park K, Lee S, Kang E, Kim K, Choi K, Kwon IC. New generation of multifunctional nanoparticles for cancer imaging and therapy. Adv Funct Mater 2009; 19: 1553–1566.

22. Janib SM, Moses AS, MacKay JA. Imaging and drug delivery using theranostic nanoparticles. Advanced Drug Deliv Rev 2010; 62(11): 1052–1063.
23. Sharon Stack M, Gray RD. Comparison of vertebrate collagenase and gelatinase using new fluorogenic substrate peptide. J Biol Chem 1989; 264(8): 4277–4281.
24. Berman J, Green M, Sugg E, Anderegg R, Millington DS, Norwood DL, McGeehan J, Wiseman J. Rapid optimization of enzyme substrates using defined substrate mixtures. J Biol Chem 1992; 267(3): 1434–1437.
25. Deng S-J, Bickett DM, Mitchell JL, Lamberti MH, Blackburn RK, Carter HL, Neugebauer J, Pahel G, Weiner MP, Moss ML. Substrate specificity of human collagenase 3 assessed using a phage-displayed peptide library. J Biol Chem 2000; 275(40): 31422–31427.
26. Delli Castelli D, Gianolio E, Geninatti Crich S, Terreno E, Aime S. Metal containing nanosized systems for MR-molecular imaging applications. Coord Chem Rev 2008; 252: 2424–2443.
27. Falvey P, Lim CW, Darcy R, Revermann T, Karst U, Giesbers M, Marcelis ATM, Lazar A, Coleman AW, Reinhoudt DN, Ravoo BJ. Bilayer vesicles of amphiphilic cyclodextrins: host membranes that recognize guest molecules. Chem Eur J 2005; 11: 1171–1180.
28. Digilio G, Menchise V, Gianolio E, Catanzaro V, Carrera C, Napolitano R, Fedeli F, Aime S. Exofacial protein thiols as a route for the internalization of Gd(III)-based complexes for MRI cell labelling. J Med Chem 2010; 53: 4877–4890.
29. Carrera C, Digilio G, Baroni S, Burgio D, Consol S, Fedeli F, Longo D, Mortillaro A, Aime S. Synthesis and characterization of a Gd(III) based contrast agent responsive to thiol containing compounds. Dalton Trans 2007; (43): 4980–4987.
30. Geninatti Crich S, Cabella C, Barge A, Belfiore S, Ghirelli C, Lattuada L, Lanzardo S, Mortillaro A, Tei L, Visigalli M, Forni G, Aime S. In vitro and in vivo magnetic resonance detection of tumor cells by targeting glutamine transporters with Gd-based probes. J Med Chem 2006; 49: 4926–4936.
31. De Leòn-Rodrìguez LM, Ortiz A, Weiner AL, Zhang S, Kovacs Z, Kodadek T, Sherry AD. Magnetic resonance imaging detects a specific peptide–protein binding event. J Am Chem Soc 2002; 124: 3514–3515.
32. Aime S, Botta M, Terreno E. Gd(III)-based contrast agents for MRI. Adv Inorg Chem 2005; 57: 173–237.
33. Caravan P, Ellison JJ, McMurry TJ, Lauffer RB. Gadolinium(III) Chelates as MRI contrast agents: structure, dynamics, and applications. Chem Rev 1999; 99: 2293–2352.
34. Kielar F, Tei L, Terreno E, Botta M. Large relaxivity enhancement of paramagnetic lipid nanoparticles by restricting the local motions of the Gd^{III} Chelates. J Am Chem Soc 2010; 132: 7836–7837.
35. Zhang Z, Greenfield MT, Spiller M, McMurry TJ, Lauffer RB, Caravan P. Multilocus binding increases the relaxivity of protein-bound MRI contrast agents. Angew Chem Int Edn 2005; 44: 6766–6769.
36. Aime S, Chiaussa M, Digilio G, Gianolio E, Terreno E. ^{1}H and ^{17}O NMR relaxometric investigations on two gadolinium(III) DTPA-like chelates endowed with high binding affinity to human serum albumin. J Biol Inorg Chem (JBIC) 1999; 4: 766–774.
37. Rasmussen HS, McCann PP. Matrix Metalloproteinase inhibition as a novel anticancer strategy: a review with special focus on batimastat and marimastat. Pharmacol Ther 1997; 75: 69–75.
38. Galardy RE, Cassabonne ME, Giese C, Gilbert JH, Lapierre F, Lopez, Schaeffer ME, Stack R, Sullivan M, Summers B, Tressler R, Tyrrell D, Wee J, Allen SD, Castellot JJ, Barletta JP, Schultz GS, Fernandez LA, Fisher S, Cui T-Y, Foellmer HG, Grobelny D, Holleran WM. Low molecular weight inhibitors in corneal ulceration. Ann NY Acad Sci 1994; 732: 315–323.
39. Watt AP. Mast cells and peptide induced histamine release. Immunopharmacology 2002; 9: 421–434.
40. Digilio G, Bracco C, Barbero L, Chicco D, Del Curto MD, Esposito P, Traversa S, Aime S. NMR Conformational analysis of antide, a potent antagonist of the gonadotropin releasing hormone. J Am Chem Soc 2002; 124: 3431–3442.
41. Nicolle GM, Merbach AE. Destruction of perfluoroalkyl surfactant aggregates by β-cyclodextrin. Chem Commun 2004; (7): 854–855.
42. Meding J, Urich M, Licha K, Reinhardt M, Misselwitz B, Fayad ZA, Weinmann H-J. Magnetic resonance imaging of atherosclerosis by targeting extracellular matrix deposition with gadofluorine M. Contrast Media Mol Imag 2007; 2: 120–129.